NASA/CR-97- 207189

S-57788-2

IN-89-CR
065203

From Top to Bottom - the Multiwavelength Campaign of V824 Ara (HD 155555)

Robert Dempsey[1], James Neff[2] Klaus Strassmeier[3], Jeffrey Linsky[4], Jeremy Lim[5], J-F. Donati[6], Fred Walter[2], Edwin Budding[7], Fred Marang[8], Ian Jordan[9], Stan Walker[9], David G. Downing[9], Doug Inwood[9], Orlon Petterson[9]

1. Introduction

A great deal of progress has been made in recent years in decomposing the 2-D structure in the atmospheres of late-type stars. Doppler images of many photospheres - single stars, T Tauri stars, Algols, RS CVn binaries to name a few - are regularly published (Strassmeier 1996; Richards & Albright 1996; Rice & Strassmeier 1996; Kürster et al. 1994). Ultraviolet spectral images of chromospheres appear in the literature (e.g., Walter et al. 1987; Neff et al. 1989) but are less common owing to the difficult nature of obtaining complete phase coverage. Zeeman doppler images of magnetic fields are now feasible (e.g., Donati et al. 1992). Performing Doppler imaging of the same targets over many seasons has also been accomplished (e.g, Vogt et al. 1997). Even when a true image reconstruction is not possible due to poor spectral resolution, we can still infer a great deal about spatial structure if enough phases are observed. However, it is increasingly apparent that to make sense of recent results, many different spectral features spanning a range of formation temperature and density must be observed *simultaneously* for a coherent picture to emerge.

Here we report on one such campaign. In 1996, we observed the southern hemisphere RS CVn binary V824 Ara (P=1^d.68, G5IV+K0V-IV) over one complete stellar rotation with the Hubble Space Telescope and EUVE. In conjunction, radio and optical photometry and spectroscopy were obtained from the ground. Unique to this campaign is the complete phase coverage of a number

[1]Space Telescope Science Institute

[2]State University of New York, Stony Brook

[3]University of Vienna

[4]Joint Institute for Laboratory Astrophysics

[5]Center for Astrophysics and Space Astronomy

[6]Observatoire de Meudon

[7]Central Institute of Technology

[8]South African Astronomical Observatory

[9]New Zealand

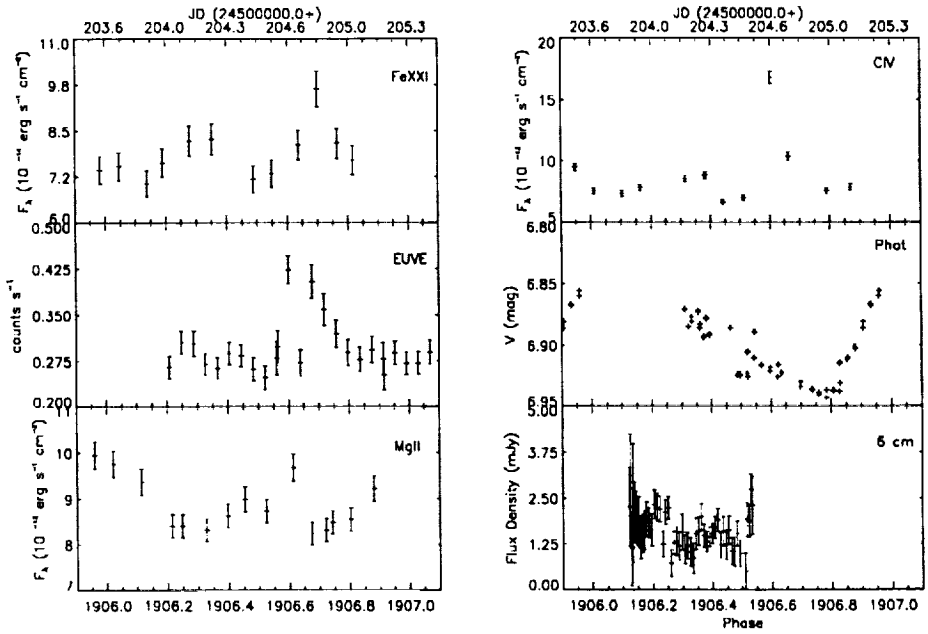

Figure 1. Extracted light curves for observations obtained simultaneously with those of HST, except for the photometric data. The displayed photometry is a folded light curve obtained from before, during, and after the HST data but little evolution is observed. Phases are computed according to the orbit computed by Pasquini et al. (1991) and phase 1906.25 corresponds to conjunction with the K star in front.

of activity proxy indicators that cover source temperatures ranging from the photosphere to the corona.

2. Observations

Extracted light curves for the interval centered on the HST observations (except for the photometry) is given in Fig. 1. A flare event is observed near phase $\phi = 1906.6$ (Fig. 2). During the observing campaign the following observations were obtained:

- **HST** - In all, some 48,000 spectra were obtained with the Goddard High Resolution Spectrograph (GHRS), mostly centered on the 1354 Å region in RAPID ($\sim$ 1 second exposure) mode. The 1354 Å spectral region contains the Fe XXI emission line which has been identified by Maran et al. (1994) as coronal in nature ($T \sim 10^7$K). All rapid readout spectra were analyzed individually to search for flares and then summed into 11 spectra. One high resolution, high S/N ACCUM spectra was also obtained of the 1354 Å region for comparison. See Fig. 3. Spectra covering the Mg II h- and k-lines and the C IV doublet were obtained at 15 and 12 phases, respectively, in ACCUM mode.

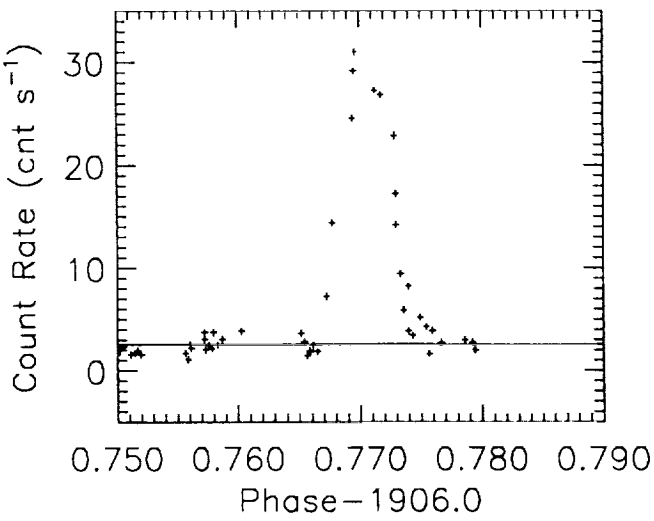

Figure 2. Count rate in the Fe XXI spectrum (entire range) as a function of phase. The dark count rate, based on theoretical models computed as a function of latitude and longitude, has been removed. The solid line indicates the mean level obtained outside of the flare.

- **EUVE** - V824 Ara was observed by EUVE for 44ksec simultaneously with the HST using the Short (SW), Medium (MW), Long (LW) wavelength, and DS detectors. Due to the (shortened) exposure time, only the Fe XVIII (93.93 Å) and Fe XXIII+Fe XX (132.8 Å) features were reliably detected, although other transitions may be marginally measurable.

- **CTIO** - Optical spectroscopy for Doppler imaging was obtained with the 1.5m telescope using a 2048x2048 chip in echelle mode. Each observation covered the He I (D3), Na I (D), Ca I (6439 Å), Fe I (6546 Å), Hα, Fe I (6663 Å), Li I (6707 Å), Ca I (6717 Å), and TiO (7055 Å) absorption features.

- **AT** - Observations at 3 and 6 cm were obtained with the Australian Telescope over a 5 day period when the target was visible from the ground.

- **Photometry** - Optical Johnson photometry were obtained at three sites, using either single-channel photometers or CCDs.

- **ESO** - Optical spectroscopy for Doppler imaging was also obtained with the ESO 1.4m CAT/CES, but not in conjunction with the core campaign. These spectra employed a 2688x512 Loral CCD with a resolution of $\approx$ 70,000 and covered the 6425–6445 Å region.

3. Ultraviolet Line Profiles

Initial spectral imaging studies of UV transitions (Walter et al. 1987, Neff et al. 1989) assumed that the intrinsic profiles could be modeled as gaussians. However, with the advent of GHRS, it became clear that simple gaussians are insufficient since very broad wings are detected in the TR profiles of several

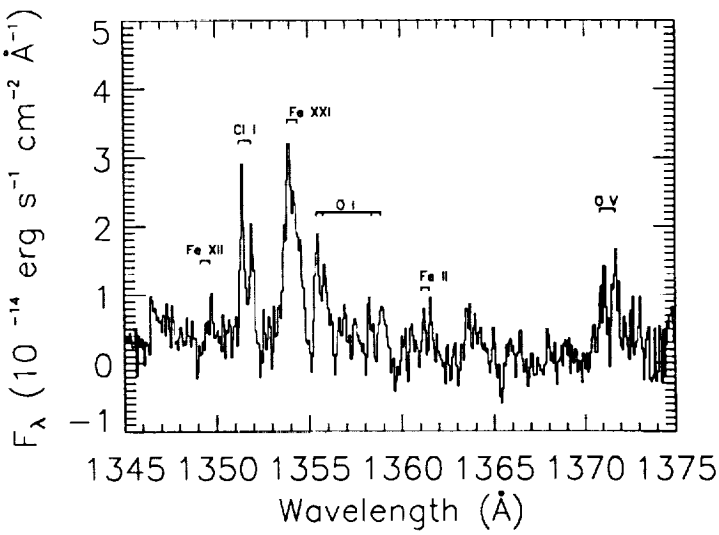

Figure 3. The Fe XXI region spectrum (ACCUM) of V824 Ara obtained near $\phi = 1906.4$ with key features identified. Results from this phase are discussed in greater detail in Airapetian & Dempsey (1997).

systems (Linsky & Wood 1994, Wood et al. 1995, Dempsey et al. 1996). Two component gaussian fits were used to fit the Mg II, C IV and Si IV profiles of V711 Tau (Wood et al. 1995, Dempsey et al. 1996). Although adequate fits to the observed line profiles may be obtained in this manner, the physical interpretation of the "broad" and "narrow" components is not clear. Wood et al. (1995) suggested that the broad component arises from microflares and Wood et al. (1997) derive a correlation between the width of this component in the C IV lines and the stellar X-ray flux. Dempsey et al. (1996) noted however, that, frequently, no unique decomposition could be obtained, making the derived widths somewhat arbitrary.

3.1. Two Gaussian Component Model

As in other late-type stars, the Mg II and C IV profiles for both stars in the V824 Ara system show very broad wings. Extended wings are also observed in at least the G-star component of He II. Initially, the profiles were modeled with 2 gaussians - one broad and one narrow. Fitting was performed using the Marquardt method (Bevington 1992) and included the GHRS PSF. However, it quickly became clear that the Mg II profiles differed in several key characteristics from those of the similar RS CVn binary, V711 Tau (HR 1099). A sample 2 component fit is shown in the top panel of Fig. 4. Free parameters in each component are the gaussian width, peak intensity and central position, for a total of 6 for each profile. In this fit, the gaussians parameters were allowed to vary in order to obtain the best fit. Note that, in this case, the broad component of the G-star completely swamps the narrow component, unlike models for the K-star component and other stars (see Wood et al. 1995, Dempsey et al. 1996). Furthermore, considerable variability is observed in the relative strengths of the 2 components at other phases; at several phases the intensity of the G-star narrow component is greater than that for the broad feature.

3.2. Anisotropic Macroturbulence Model

In order to try to improve on the model we applied the anisotropic turbulence (AT) model presented in Gray (1992). In this case, the line profile's shape results from the relative contribution of a radial macroturbulent velocity distribution ($\Theta_R(V_R)$) with fractional covering area A_R, and a tangential or horizontal distribution ($\Theta_T(V_T)$), covering area A_T. The distributions are assumed to be gaussian for a given $V_{R,T}$ while A_T is taken to be $1.0 - A_R$. The observed flux is then the standard convolution

$$F_\nu = \int I_\nu^o * (A_R\Theta_R(V_R) + A_T\Theta_T(V_T))cos\theta d\omega \qquad (1)$$

integrated over the entire disk. The intrinsic line profile, I_ν^o, includes microturbulence (ξ), the rotational velocity (v $sini$), and linear limb brightening/darkening with coefficient ϵ. The PSF was included and again we used the Marquardt method of minimization. For each model, the central position (λ_{meas}), V_R, V_T, and peak intensity are free parameters for a total of 4 for each profile. Although ξ could be varied as well, little improvement is made in doing so. We used $\xi = 12$ km s^{-1}. In our models, $\epsilon = -0.2$. The results are shown in the lower panel of Fig. 4.

A comparison between the two models is given in Tables 1 & 2. Although the radial component dominates the profile, the tangential contribution is needed to fit the extended wings. Both fits have χ^2 around 0.10 and are very similar in quality, although the wings are fit slightly better in the AT model. Similar results are found for the Mg II k-line.

Finally, we applied the AT model to the $\phi = 2.73$ Mg II spectra of V711 Tau (see Dempsey et al. 1996) and list the results in Table 2 as well. Note that the velocities are significantly larger than we find for V824 Ara and the G star model profiles have no tangential contribution. This is consistent with the results of Robinson et al. (1996), who found that atmospheric turbulence was detected in all UV emission lines of V711 Tau and is anisotropically distributed purely along the radial or tangential direction (ignoring limb darkening).

These results suggest that anisotropic velocity distributions, perhaps generated by non-linear Alfvén waves, can produce the observed line profiles rather than heating by microflares. It is also the case that there are fundamental differences in the atmospheres of V824 Ara and V711 Tau. Analysis of the C IV, Si IV, O V, Fe XXI and He II profiles will allow us to map out the velocity structure throughout the atmosphere of V824 Ara and any changes as a function of phase.

Acknowledgments. KGS is supported by FWF grant S-7302.

References

Airapetian, V. & Dempsey, R. C. 1997, these proceedings

Bevington, P. R., 1992, Data Reduction and Error Analysis for the Physical Science (McGraw-Hill: New York)

Dempsey, R. C., Neff, J. E., Thorpe, M. J., Linsky, J. L., Brown, A., Cutispoto, G., & Rodonó, M. 1996, ApJ, 470, 1172

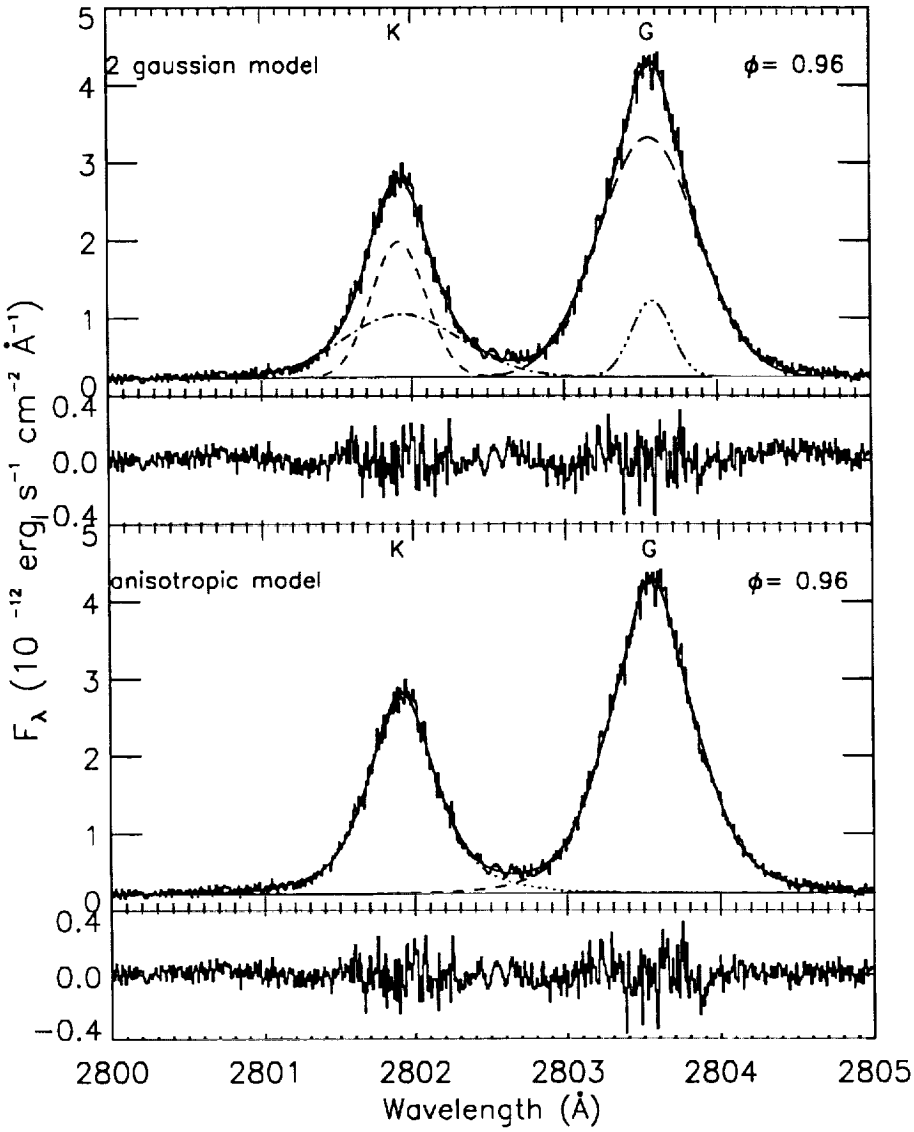

Figure 4. The Mg II h profile at $\phi = 1906.96$ showing the best fit two gaussian component model and AT model. Residuals from the models are shown below each fit. For ease of fitting and visualization, the interstellar line has been approximately subtracted using 3 gaussians. For the AT model, *vsini* was taken to be 29 & 37 km s^{-1} for the K and G stars, respectively.

Donati, J.-F., Brown, S. F., Semel, M., Rees, D. E., Dempsey, R. C., Matthews, J. M., Henry, G. W. & Hall, D. S. 1992, 265, 682

Gray, D. 1992, in The Observation, & Analysis of Stellar Photospheres, (cambridge Univ. Press: New York), p407

Kürster, M, Schmitt, J, H. M. M. & Cutispoto, G. 1994, A&A, 289, 899

Linsky, J. L., & Wood, B. E. 1994, ApJ, 430, 342

Maran, S. P., et al. 1994, ApJ, 421, 800

Neff, J. E., Walter, F. M., Rodonò, M. & Linsky, J. L. 1989, A&A215, 79

Pasquini, L., Cutispoto, G. Gratton, R. & Mayor, M. 1991, A&A, 248, 72

Robinson, R., Airapetian, V., Maran, S. P., & Carpenter, K. G. 1996, ApJ, 469, 872

Rice, J. B. & Strassmeier, K. 1996, A&A, 316, 164

Richards, M. & Albright, G. 1996, in *Stellar Surface Structure*, ed. K. G. Strassmeier & J. L. Linsky, p 493

Strassmeier, K., G. 1996, A&A, 314, 558

Walter, F. M., Neff, J. E., Gibson, D. M., Linsky, J. L., Rodonó, M., Gary, D. E. & Butler, C. J. 1987, A&A186, 241

Wood, B. E., Harper, G. M., Linsky, J. L. & Dempsey, R. C. 1995, ApJ, 458, 761

Wood, B. E., Linsky, J. L. & Ayres, T. R. 1997, ApJ, 478, 745

Vogt et al., 1997, ApJS, submitted

Table 1. 2 gaussian model

Comp.	λ_{meas} Å	ΔV^a km s^{-1}	Width^b km s^{-1}	FWHM km s^{-1}	F_λ 10^{-12} erg s^{-1} cm^{-2}
K (narrow)	2801.916	-2.8	33.9 ± 3.3	78.0 ± 7.6	0.80 ± 0.03
K (broad)	2801.934	-4.8	73.0 ± 10.5	170.0 ± 24.4	0.80 ± 0.07
G (narrow)	2803.570	-8.1	24.4 ± 4.0	55.7 ± 9.1	0.32 ± 0.01
G (broad)	2803.552	-6.2	60.4 ± 2.0	140.7 ± 4.6	2.50 ± 0.03

[a]Radial velocity with respect to predicted orbital position.

[b]Gaussian width.

Table 2. AT model

Comp.	λ_{meas} Å	ΔV^a km s^{-1}	V_R km s^{-1}	V_T km s^{-1}	A_R	F_λ 10^{-12} erg s^{-1} cm^{-2}
			V824 Ara Mg II h-line ϕ = 1906.96			
K0V-IV	2801.916	-2.9	33.6 ± 4.4	94.8 ± 11.8	0.80 ± 0.03	1.60
G5IV	2803.558	-6.7	45.0 ± 3.2	95.0 ± 9.5	0.85 ± 0.02	2.89
			V824 Ara Mg II k-line ϕ = 1906.96			
K0V-IV	2794.734	-0.5	44.1 ± 3.3	75.9 ± 10.4	0.88 ± 0.02	1.89
G5IV	2796.376	5.2[b]	51.7 ± 2.2	129.3 ± 7.0	0.84 ± 0.01	3.79
			V711 Tau Mg II h-line ϕ = 2.73[c]			
K1IV	2802.140	-4.6	100.2 ± 0.1	193.2 ± 0.5	0.98 ± 0.00	2.14
G5IV	2803.180	5.7	29.4 ± 0.1	...	1.00 ± 0.00	0.17
			V711 Tau Mg II k-line ϕ = 2.73[c]			
K1IV	2794.970	-3.9	118.0 ± 0.1	181.0 ± 0.2	0.98 ± 0.00	2.91
G5IV	2795.920	-4.4	48.1 ± 0.1	...	1.00 ± 0.00	0.32

[a]Radial velocity with respect to predicted orbital position.
[b]Contaminated by the Mg II subordinate line at 2797.998 Å.
[c]Here ξ = 15.9 km s^{-1}, left as free parameter.